Supplementary material

Capillary-Flow Dynamics in Open Rectangular Microchannels

Panayiotis Kolliopoulos, Krystopher S. Jochem, Daniel Johnson, Wieslaw J. Suszynski, Lorraine F. Francis, and Satish Kumar[1]

Department of Chemical Engineering and Materials Science, University of Minnesota, Minneapolis, MN 55455, USA

This document provides supplementary material on the governing equations and the method for calculating the rescaled cross-sectional-averaged dimensionless velocities $\bar{w}_i$ used in the primary article "Capillary-Flow Dynamics in Open Rectangular Microchannels".

S1 Governing Equations

We consider mass and momentum conservation of an incompressible Newtonian liquid with constant density, given by

$$\tilde{\boldsymbol{\nabla}} \cdot \tilde{\boldsymbol{u}} = 0, \tag{S1a}$$

$$\rho\left[\frac{\partial \tilde{\boldsymbol{u}}}{\partial \tilde{t}} + (\tilde{\boldsymbol{u}} \cdot \tilde{\boldsymbol{\nabla}})\tilde{\boldsymbol{u}}\right] = -\tilde{\boldsymbol{\nabla}}\tilde{p} + \mu\tilde{\nabla}^2\tilde{\boldsymbol{u}} + \rho\tilde{\boldsymbol{g}}, \tag{S1b}$$

where $\tilde{\boldsymbol{u}} = (\tilde{u}, \tilde{v}, \tilde{w})$ is the velocity field in Cartesian coordinates, $\tilde{p}$ is the liquid pressure, and $\tilde{\boldsymbol{g}} = (\tilde{g}_x, \tilde{g}_y, \tilde{g}_z)$ is the gravitational acceleration. The no-slip and no-penetration conditions are applied along the solid walls as

$$\tilde{\boldsymbol{u}} = 0. \tag{S2}$$

The boundary conditions for the normal and tangential stresses at the liquid-air interface $\tilde{h}(\tilde{x}, \tilde{z}, \tilde{t})$ are given by

$$[\![\boldsymbol{n} \cdot \tilde{\boldsymbol{T}} \cdot \boldsymbol{n}]\!] = \sigma(\tilde{\boldsymbol{\nabla}}_s \cdot \boldsymbol{n}), \tag{S3a}$$

$$[\![\boldsymbol{t}_1 \cdot \tilde{\boldsymbol{T}} \cdot \boldsymbol{n}]\!] = 0, \tag{S3b}$$

$$[\![\boldsymbol{t}_2 \cdot \tilde{\boldsymbol{T}} \cdot \boldsymbol{n}]\!] = 0. \tag{S3c}$$

Here, $\tilde{\boldsymbol{T}} = -\tilde{p}\boldsymbol{I} + \mu[\tilde{\boldsymbol{\nabla}}\tilde{\boldsymbol{u}} + (\tilde{\boldsymbol{\nabla}}\tilde{\boldsymbol{u}})^T]$ is stress tensor, $\boldsymbol{I}$ is the identity tensor, $\tilde{\boldsymbol{\nabla}}_s = \tilde{\boldsymbol{\nabla}} - \boldsymbol{n}(\boldsymbol{n} \cdot \tilde{\boldsymbol{\nabla}})$ is the surface gradient operator, $\boldsymbol{n}$ is the unit outward normal vector, and $\boldsymbol{t}_1$, $\boldsymbol{t}_2$ are the two

[1]kumar030@umn.edu

tangent vectors at the interface in the transverse and axial directions, respectively. These vectors are given by

$$\boldsymbol{n} = \frac{1}{[1+(\partial_{\tilde{x}}\tilde{h})^2+((\partial_{\tilde{z}}\tilde{h})^2]^{1/2}}(-\partial_{\tilde{x}}\tilde{h}, 1, -\partial_{\tilde{z}}\tilde{h}), \tag{S4a}$$

$$\boldsymbol{t}_1 = \frac{1}{[1+((\partial_{\tilde{x}}\tilde{h})^2]^{1/2}}(1, \partial_{\tilde{x}}\tilde{h}, 0), \tag{S4b}$$

$$\boldsymbol{t}_2 = \frac{1}{[1+((\partial_{\tilde{z}}\tilde{h})^2]^{1/2}}(0, \partial_{\tilde{z}}\tilde{h}, 1). \tag{S4c}$$

Equations (S1a) and (S1b) are rendered dimensionless using the following scalings

$$(\tilde{x}, \tilde{y}, \tilde{z}) = (Hx, Hy, Lz), \qquad \tilde{t} = \frac{L}{U}t, \qquad \tilde{p} = \frac{\mu U}{\epsilon H}p,$$
$$(\tilde{u}, \tilde{v}, \tilde{w}) = (\epsilon U u, \epsilon U v, U w), \qquad \epsilon = \frac{H}{L}, \qquad U = \frac{2\epsilon\sigma}{\mu}.$$

Additionally, the gravitational acceleration vector is scaled as $(\tilde{g}_x, \tilde{g}_y, \tilde{g}_z) = (gg_x, gg_y, gg_z)$ where g is the magnitude of the gravitational acceleration. The dimensionless parameters that arise are the Reynolds number $Re = \rho UH/\mu$ (ratio of inertial to viscous forces), the capillary number $Ca = \mu U/\epsilon\sigma$ (ratio of viscous to surface-tension forces), and the Bond number $Bo = \rho g H^2/\sigma$ (ratio of gravitational to surface-tension forces).

Using these scalings, (S1a) and (S1b) become

$$\frac{\partial u}{\partial x} + \frac{\partial v}{\partial y} + \frac{\partial w}{\partial z} = 0, \tag{S5a}$$

$$\epsilon^3 Re\left[\frac{\partial u}{\partial t} + u\frac{\partial u}{\partial x} + v\frac{\partial u}{\partial y} + w\frac{\partial u}{\partial z}\right] = -\frac{\partial p}{\partial x} + \epsilon^2\left[\frac{\partial^2 u}{\partial x^2} + \frac{\partial^2 u}{\partial y^2} + \epsilon^2\frac{\partial^2 u}{\partial z^2}\right] + \frac{Bo}{Ca}g_x, \tag{S5b}$$

$$\epsilon^3 Re\left[\frac{\partial v}{\partial t} + u\frac{\partial v}{\partial x} + v\frac{\partial v}{\partial y} + w\frac{\partial v}{\partial z}\right] = -\frac{\partial p}{\partial y} + \epsilon^2\left[\frac{\partial^2 v}{\partial x^2} + \frac{\partial^2 v}{\partial y^2} + \epsilon^2\frac{\partial^2 v}{\partial z^2}\right] + \frac{Bo}{Ca}g_y, \tag{S5c}$$

$$\epsilon Re\left[\frac{\partial w}{\partial t} + u\frac{\partial w}{\partial x} + v\frac{\partial w}{\partial y} + w\frac{\partial w}{\partial z}\right] = -\frac{\partial p}{\partial z} + \left[\frac{\partial^2 w}{\partial x^2} + \frac{\partial^2 w}{\partial y^2} + \epsilon^2\frac{\partial^2 w}{\partial z^2}\right] + \frac{Bo}{\epsilon Ca}g_z. \tag{S5d}$$

In the limits where $\epsilon^2 \ll 1$, $\epsilon Re \ll 1$, and $Bo/Ca \ll \epsilon$, the above equations reduce to

$$\frac{\partial u}{\partial x} + \frac{\partial v}{\partial y} + \frac{\partial w}{\partial z} = 0, \tag{S6a}$$

$$\frac{\partial p}{\partial x} = \frac{\partial p}{\partial y} = 0, \tag{S6b}$$

$$\frac{\partial p}{\partial z} = \frac{\partial^2 w}{\partial x^2} + \frac{\partial^2 w}{\partial y^2}. \tag{S6c}$$

The boundary conditions for the normal (S3a), transverse tangential (S3b), and axial tangential (S3c) stresses at the free surface reduce to

$$p = -Ca^{-1}\frac{\partial_x^2 h}{[1+(\partial_x h)^2]^{3/2}} = -Ca^{-1}\left[\frac{\partial_x h}{[1+(\partial_x h)^2]^{1/2}}\right]_x, \tag{S7a}$$

$$0 = [1-(\partial_x h)^2]\left(\frac{\partial u}{\partial y}+\frac{\partial v}{\partial x}\right) + 2\partial_x h\left(-\frac{\partial u}{\partial x}+\frac{\partial v}{\partial y}\right) - \partial_z h\left(\frac{\partial w}{\partial x}+\partial_x h\frac{\partial w}{\partial y}\right), \tag{S7b}$$

$$0 = \frac{\partial w}{\partial y} - \partial_x h\frac{\partial w}{\partial x}. \tag{S7c}$$

Based on (S6b) the $\mathcal{O}(1)$ term in p is only dependent on z and t, and thus the leading-order curvature term (term in brackets on far right of (S7a)) is actually independent of x and must only depend on z and t. The derivation of (S6) and (S7) can also be seen in Yang & Homsy (2006) and White & Troian (2019), who considered V-shaped channel cross sections.

Up to this point no assumption has been made regarding the channel cross-sectional geometry. Here, we consider two geometries for the channel cross section: (a) rectangular (figure 5a) and (b) V-shaped (figure 5b). Using these two geometries we can describe all the liquid cross sections in figures 4a and 4b in terms of the liquid height on the solid wall $a(z,t)$ and the contact angle $\theta(z,t)$. The meniscus-deformation ($a = 1$) and meniscus-recession ($\theta = \theta_0$) regimes are described using the rectangular cross section, while the corner-transition ($a = 1$) and corner-flow ($\theta = \theta_0$) regimes are described using the V-shaped cross section.

Each cross-sectional geometry requires three additional boundary conditions to obtain expressions for $p(z,t)$ and $h(x,z,t)$: the contact-line location on the solid wall, a symmetry condition, and the definition of the contact angle θ. For the rectangular channel cross section (figure 5a) these boundary conditions are

$$h = a \quad \text{at} \quad x = 1/2\lambda, \tag{S8a}$$

$$\partial_x h = 0 \quad \text{at} \quad x = 0, \tag{S8b}$$

$$\mathbf{n}\cdot\mathbf{k} = \cos\theta \quad \text{at} \quad x = 1/2\lambda, \tag{S8c}$$

where $\mathbf{k} = (-1,0,0)$ is the inward normal to the sidewall. Retaining $\mathcal{O}(1)$ terms, (S8c) reduces to $\partial_x h = \cot\theta$ at $x = 1/2\lambda$.

Similarly, for the V-shaped channel cross section (figure 5b) these boundary conditions are

$$h = a\cos\beta \quad \text{at} \quad x = a\sin\beta, \tag{S9a}$$

$$\partial_x h = 0 \quad \text{at} \quad x = \frac{a\sin\beta}{2}\left(1 - \frac{\cos(\theta_0 + \pi/2 - \beta)}{\cos(\theta + \beta)}\right), \tag{S9b}$$

$$\mathbf{n}\cdot\mathbf{k} = \cos\theta \quad \text{at} \quad x = a\sin\beta, \tag{S9c}$$

where $\beta = \arctan(\cos\theta/\cos\theta_0)$ (see §S3) and $\mathbf{k} = (-\cos\beta, \sin\beta, 0)$. Retaining $\mathcal{O}(1)$ terms, (S9c) reduces to $\partial_x h = \cot(\theta + \beta)$ at $x = a\sin\beta$.

Expressions for $p(z,t)$ and $h(x,z,t)$ as a function of the dimensionless liquid height $a(z,t)$ on the side walls and the contact angle $\theta(z,t)$ are obtained for each regime in figure 4, as described below. Equation (S7a) is integrated twice with respect to x and the boundary condition sets (S8) and (S9) are used to obtain the following $\mathcal{O}(1)$ expressions

$$\left.\begin{aligned} p &= -\lambda\cos\theta(z,t) \\ h &= 1 + \frac{\tan\theta(z,t)}{2\lambda} - \left[\frac{1}{4\lambda^2\cos^2\theta(z,t)} - x^2\right]^{1/2} \end{aligned}\right\} \quad \text{meniscus deformation,} \tag{S10a}$$

$$\left.\begin{aligned} p &= -\lambda\cos\theta_0 \\ h &= a(z,t) + \frac{\tan\theta_0}{2\lambda} - \left[\frac{1}{4\lambda^2\cos^2\theta_0} - x^2\right]^{1/2} \end{aligned}\right\} \quad \text{meniscus recession,} \tag{S10b}$$

$$\left.\begin{aligned} p &= -\frac{\cos\theta_0 - \sin\theta(z,t)}{2} \\ h &= \frac{\cos\theta(z,t)}{\cos(\theta(z,t)+\beta)} - \left[\left(\frac{\sin\beta}{\cos(\theta(z,t)+\beta)}\right)^2 - x^2\right]^{1/2} \end{aligned}\right\} \quad \text{corner transition,} \tag{S10c}$$

$$\left.\begin{aligned} p &= -\frac{\cos\theta_0 - \sin\theta_0}{2a(z,t)} \\ h &= \frac{a(z,t)\cos\theta_0}{\cos(\theta_0+\pi/4)} - \left[\left(\frac{a(z,t)\sin\pi/4}{\cos(\theta_0+\pi/4)}\right)^2 - x^2\right]^{1/2} \end{aligned}\right\} \quad \text{corner flow,} \tag{S10d}$$

where θ_0 is the equilibrium contact angle and λ is the channel aspect ratio. Equations (S10a) and (S10b) were also used by Tchikanda *et al.* (2004) and Nilson *et al.* (2006). A similar expression to (S10c) can be found in Weislogel & Nardin (2005). The expressions in (S10d) were also used by Romero & Yost (1996), Weislogel & Lichter (1998), Nilson *et al.* (2006), Yang & Homsy (2006), and White & Troian (2019). We note that to reconstruct free-surface profiles, the height profiles h in (S10c) and (S10d) corresponding to figure 5b must be rotated by angles $\beta = \arctan(\cos\theta/\cos\theta_0)$ and $\beta = \pi/4$, respectively, to match the orientation of the channel cross section in figures 4a and 4b.

S2 Velocity Field

Here, we describe the method for calculating cross-sectional-averaged dimensionless velocities $\bar{w}_D(s)$, $\bar{w}_T(s)$, and $\bar{w}_C(s)$ seen in (3.14). To calculate $\bar{w}_D(s)$ we rescale the velocity w in (S6c) with $-\partial p/\partial z$. This reduces (S6c) to

$$-1 = \frac{\partial^2 w'}{\partial x^2} + \frac{\partial^2 w'}{\partial y^2} \tag{S11a}$$

subject to

$$w' = 0 \quad \text{at solid boundaries} \tag{S11b}$$

and

$$0 = \frac{\partial w'}{\partial y} - \partial_x h \frac{\partial w'}{\partial x} \quad \text{at} \quad y = h, \tag{S11c}$$

where h is given by (S10a) and w' is the rescaled velocity. The cross-sectional-averaged dimensionless velocity $\bar{w}_D(s)$ is defined as

$$\bar{w}_D = \frac{1}{A} \int_A w' \, \mathrm{d}A. \tag{S12}$$

Equation (S11a) is solved subject to boundary conditions (S11b) and (S11c). Equation (S12) is then used to obtain $\bar{w}_D(s)$. Note that the dependence of $\bar{w}_D(s)$ on $s \in [1, s_D]$ is obtained by varying the contact angle $\theta \in [\pi/2, \theta_0]$ to create different cross sections characterized by h (figure 5a).

To calculate $\bar{w}_T(s)$ and $\bar{w}_C$, we rescale the velocity w in (S6c) with $-a^2\partial p/\partial z$, and x, y with a. This reduces (S6c) to

$$-1 = \frac{\partial^2 w'}{\partial (x')^2} + \frac{\partial^2 w'}{\partial (y')^2} \tag{S13a}$$

subject to

$$w' = 0 \quad \text{at solid boundaries} \tag{S13b}$$

and

$$0 = \frac{\partial w'}{\partial y'} - \frac{\partial h'}{\partial x'} \frac{\partial w'}{\partial x'} \quad \text{at} \quad y = h'. \tag{S13c}$$

The rescaled interface height is $h' = h/a$, where h is given by (S10c) and (S10d) for the corner-transition and corner-flow regimes, respectively, and x' and y' are the rescaled x and y coordinates. The cross-sectional-averaged dimensionless velocities $\bar{w}_T(s)$ and $\bar{w}_D$ are defined as

$$\bar{w}_i = \frac{1}{A'(\theta, \theta_0)} \int_{A'(\theta,\theta_0)} w' \, \mathrm{d}A', \quad \text{for} \quad i = T, C, \tag{S14}$$

where $A'(\theta,\theta_0) = \hat{B}(\theta,\theta_0)/(\cos\theta_0 - \sin\theta)^2$ for the corner-transition regime and $A'(\theta = \theta_0,\theta_0) = 2\hat{A}(\theta_0)/(\cos\theta_0 - \sin\theta_0)^2$ for the corner-flow regime (see (3.12c) and (3.12d)).

Equation (S13a) is solved subject to boundary conditions (S13b) and (S13c). Equation (S14) is then used to obtain $\bar{w}_T(s)$ and $\bar{w}_C$. Note that the dependence of $\bar{w}_T(s)$ on $s \in [s_T, s_C]$ is obtained by varying the contact angle $\theta \in [\theta_T, \theta_0]$ to create different cross sections characterized by h (figure 5b). Because the rescaled cross-sectional area $A'(\theta_0,\theta_0) = \hat{A}(\theta_0)/(\cos\theta_0 - \sin\theta_0)^2$ is constant in the corner-flow regime, (S13a) only needs to be solved once to obtain $\bar{w}_C$ for a given θ_0.

S3 Interior angle β

Here, we derive the expression relating β (found in figure S1 and (S10c)) to the equilibrium contact angle θ_0 at the channel bottom and the contact angle θ on the channel side wall as depicted in figure S1. Initially, we focus on $\triangle OAB$ and $\triangle OCB$ to obtain

$$\gamma_1 = \pi/2 - \beta - \theta \quad \text{and} \quad \gamma_2 = \beta - \theta_0. \tag{S15}$$

We then consider $\triangle OAD$ and $\triangle OCE$ where

$$\sin\gamma_1 = \frac{\overline{AD}}{\overline{OA}} = \frac{a\sin\beta}{r} \quad \text{and} \quad \sin\gamma_2 = \frac{\overline{CE}}{\overline{OC}} = \frac{a_0\cos\beta}{r}. \tag{S16}$$

Here, r is the radius of the circular-arc meniscus. The expressions in (S16) are then used to relate the contact line positions a_0 and a for the channel bottom and side wall through

$$a_0 = \frac{a\tan\beta\sin\gamma_2}{\sin\gamma_1}. \tag{S17}$$

Next, we consider $\overline{OB}$ where

$$\overline{OE} + \overline{EB} = \overline{OD} + \overline{DB} \Leftrightarrow \frac{a_0\cos\beta}{\tan\gamma_2} + a_0\sin\beta = \frac{a\sin\beta}{\tan\gamma_1} + a\cos\beta. \tag{S18}$$

Finally, we use (S15) and (S17) in (S18) to obtain

$$\beta = \arctan\left(\frac{\cos\theta}{\cos\theta_0}\right). \tag{S19}$$

A similar expression can be found in Weislogel & Nardin (2005).

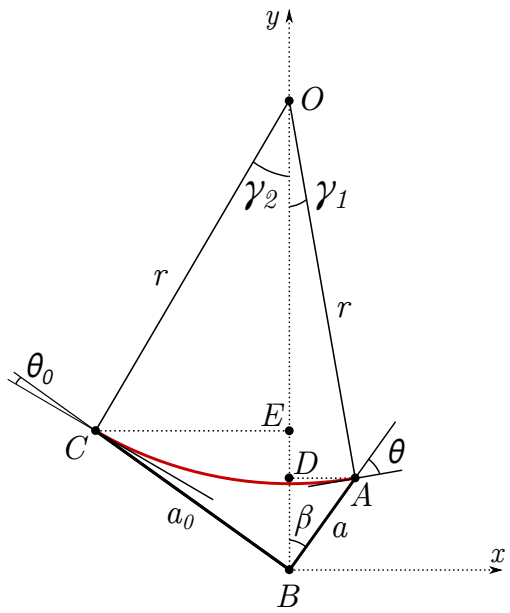

Figure S1: Cross-sectional schematic for corner-transition ($a = 1$) and corner-flow ($\theta = \theta_0$) regimes.

References

Nilson, R. H., Tchikanda, S. W., Griffiths, S. K. & Martinez, M. J. 2006 Steady evaporating flow in rectangular microchannels. *Int. J. Heat Mass Transf.* **49** (9–10), 1603–1618.

Romero, L. A. & Yost, F. G. 1996 Flow in an open channel capillary. *J. Fluid Mech.* **322**, 109–129.

Tchikanda, S. W., Nilson, R. H. & Griffiths, S. K. 2004 Modeling of pressure and shear-driven flows in open rectangular microchannels. *Int. J. Heat Mass Transf.* **47** (3), 527–538.

Weislogel, M. M. & Lichter, S. 1998 Capillary flow in an interior corner. *J. Fluid Mech.* **373**, 349–378.

Weislogel, M. M. & Nardin, C. L. 2005 Capillary driven flow along interior corners formed by planar walls of varying wettability. *Microgravity Sci. Technol.* **17** (3), 45–55.

White, N. C. & Troian, S. M. 2019 Why capillary flows in slender triangular grooves are so stable against disturbances. *Phys. Rev. Fluids* **4** (5), 1–29.

Yang, L. & Homsy, G. M. 2006 Steady three-dimensional thermocapillary flows and dryout inside a V-shaped wedge. *Phys. Fluids* **18** (4), 042107.